Scientific Visualization, 2024, volume 16, number 2, pages 11 - 22, DOI: 10.26583/sv.16.2.02

Shadow Detection and Elimination for Robot and Machine Vision Applications

Luma Issa Abdul-Kreem[1,A], Hussam k. Abdul-Ameer[2,B]

[A] Control and Systems Engineering Departament, University of Technology, Baghdad, Iraq
[B] Biomedical Engineering Departament, University of Baghdad, Al-Khwarizmi College of Engineering, Baghdad, Iraq

[1] ORCID: 0000-0002-6161-2428, luma.i.abdulkreem@uotechnology.edu.iq
[2] ORCID: 0000-0001-6799-3201, hussam@kecbu.uobaghdad.edu.iq

Abstract

Shadow removal is crucial for robot and machine vision as the accuracy of object detection is greatly influenced by the uncertainty and ambiguity of the visual scene. In this paper, we introduce a new algorithm for shadow detection and removal based on different shapes, orientations, and spatial extents of Gaussian equations. Here, the contrast information of the visual scene is utilized for shadow detection and removal through five consecutive processing stages. In the first stage, contrast filtering is performed to obtain the contrast information of the image. The second stage involves a normalization process that suppresses noise and generates a balanced intensity at a specific position compared to the neighboring intensities. In the third stage, the boundary of the target object is extracted, and in the fourth and fifth stages, respectively, the region of interest (ROI) is highlighted and reconstructed. Our model was tested and evaluated using realistic scenarios which include outdoor and indoor scenes. The results reflect the ability of our approach to detect and remove shadows and reconstruct a shadow free image with a small error of approximately 6%.

Keywords: Shadow Distribution Visualization, Spatial Analysis of Shadows, Filtered Data Visualization, Data Normalization, Shadow Removal, Machine and Robot Vision.

1. Introduction

Shadows pose a problem in robot, machine, and computer vision in general. Shadows share movement and shape with the related object, and as a consequence, confusion occurs due to object detection or obstacle avoidance. Although shadows can help interpret a visual scene such as image intensity and object configuration ([1], [2]), shadows corrupt many applications such as object monitoring, objects recognition, and image decomposition ([3]- [5]). In the literature, shadows have been classified as self-shadows and cast shadows, in which object projections on the background are denoted as cast shadows, on the other hand, the shadow projection on the object itself is referred to as a self-shadow ([6] [7] [8]).

Many approaches have been suggested for shadow detection and removal. These approaches have addressed the problem of shadows in different applications (see, [9]-[10]). In the studies by ([11]-[12]), the authors show the unfavourable influence of shadows in the visual scene of an agricultural robot. They suggest using image segmentation algorithms, ultrametric contour maps, and machine learning techniques to remove shadows from an image. Several researchers, on the other hand, have assessed the authenticity of an image by removing the incorrect shadows in the edited images (see for example, [13]). These studies have investigated the effects of shadows in detecting forgeries by revealing the inconsistencies in an image, such as the coherence between the shadows and light direction (see, [14] and [15].

Several works have concentrated on a fine-grained analysis of colour distributions in an image. In [16], the authors suggested combining an edge conditional random field (CRF) to classify edges in consumer photographs. A related method presented by [17] considers a moving viewpoint by comparing variant and invariant shadow features. These features primarily comprised colour, texture, edge which were then embedded into a segmentation pipeline that provides predictions of the shadow status.

Many studies (for example [18]-[19], [13] and) use neural networks and learning-based algorithms for shadow detection and removal. These algorithms require learning regarding both the images that contain shadows, as well as the corresponding images that do not contain shadows (i.e., for a specific scene, two images need to be taken in which one contains a shadow and the other does not). Consequently, these algorithms require a training process with a large number of images with different cases (see, [20]).

As the shadow region in most cases involves gradual changes in luminance, some researchers tend to use the gradient-based algorithm for shadow removal (see [21]). This an algorithm assumes that the intensity of the shadow regions changes gradually, and as a consequence, this algorithm fails if the shadow has a sharp texture [8].

Shadow detection and removal has two main challenges: how the shadow region can be detected accurately in a complex scene, and how the shading can be removed yet keeping the details and information of the region and without defecting the boundaries of the objects (see, [22], [23]). In essence, shadows are a critical issue for object recognition systems and require further investigation and development. In this work, the distribution of intensity for an object along with its shadow is visualized and analyzed to eliminate the shadow's intensity effect using various types of data filtering. We propose an algorithm that handles real-world shadows and removes them. This algorithm consists of five consecutive processing stages. In the first stage, contrast information is detected using Gaussian derivative functions along the x and y directions. In the second stage, the contrast information is normalized to generate a balanced activity at a specific position in relation to neighboring activities. Moving to the third stage, the boundary of the (ROI) for the target object is extracted. Subsequently, in the fourth and fifth stages, the interior of the detected object is highlighted and reconstructed, respectively. This algorithm can be used in different applications, such as robot and machine vision. Unlike the state-of-art approaches ([13] and [24], [25]) for shadow detection and removal, our algorithm does not require a training process on different shadows and shadowless images. Our mechanism reconstructs a target object in a shadowless image through five stages using Gaussian equations with different shapes and orientations.

The rest of the paper is structured as follows. Section 2 introduces the suggested methodology for shadow detection and removal. The discussion and experimental results of the proposed algorithm are presented in Section 3. Finally, Section 4 presents the conclusions and summarizes the contribution of this work.

2. Shadow Elimination Approach

In this work, we detect and eliminate the shadow of an image using five consecutive stages. The first stage involves achieving contrast filtering information of the image by utilizing the first-order derivative of the Gaussian function along the x and y axes. This information is then normalized in the second stage. In the third stage, we extract the shadowless boundary of the target object. Moving to the fourth stage, we highlight the obtained enclosed region of the object contour. Finally, in the fifth stage, we use this region to reconstruct the object in the visual scene without any shadow. Fig. 1 presents the linear scheme of the suggested approach. In the following subsections, we provide detailed descriptions of each stage.

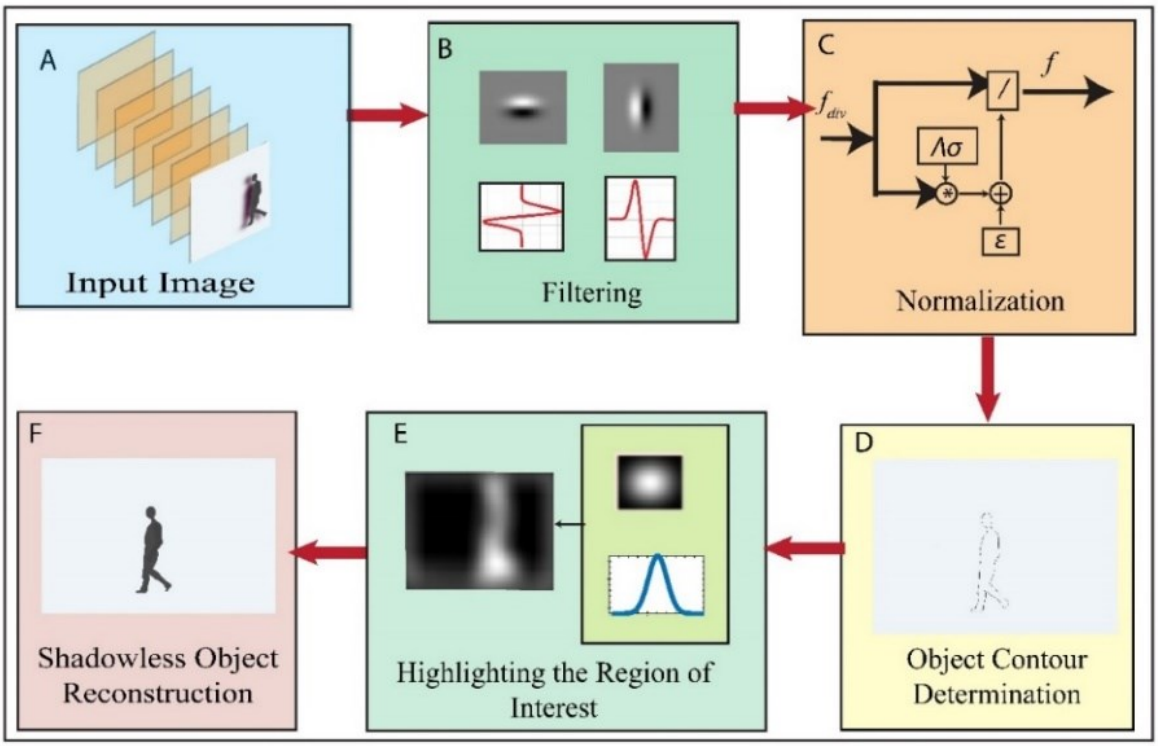

Fig.1 The linear scheme of suggested approach.

2.1. Contrast Filtering

In this stage, the object in the visual scene is detected based on contrast information of the Gaussian derivative functions along x and y directions. The first-order derivative of the Gaussian function in 2D (x,y) space is defined by

$$f_{div} = \sqrt{(I * g_x)^2 + \left(I * g_y\right)^2},$$

where (I) represents the input image and * denotes the spatial convolution operator, g_x and g_y denote Gaussian derivative kernels along x and y directions, respectively. Since an object edge is an elongated change in the spatial domain, we propose using the derivative function of an elongated Gaussian kernel. The first stage of Fig.1 shows the kernels of the 2D spatial derivative of the Gaussian function. The partial derivatives are thus calculated by

$$g_x = (-x/\sigma_x^2) \cdot \Lambda_{\sigma x_1, \sigma y_1}$$
$$g_y = \left(-y/\sigma_y^2\right) \cdot \Lambda_{\sigma x_2, \sigma y_2}$$

where $\Lambda\sigma x_1$,σy_1 and $\Lambda\sigma x_2$, σy_2 represent Gaussian functions with 2D spatial extent (σx_1, σy_1) and ($\sigma x_2, \sigma y_2$) in x and y directions, respectively.

2.2. Normalization

In order to suppress noise and achieve a balanced intensity response in the spatial domain, we normalize the response of each location based on the relevant neighbourhoods (see [26], [27]). The normalization process is thus defined by

$$f = f_{\text{div}} / (\varepsilon + f_{\text{div}^* \Lambda\sigma})$$

where ε represents a small value to prevent the equation from zero division and Λ represents a fall-off function that weights the intensity of the spatial neighbourhoods of the target position in the image based on the spatial extent σ.

2.3. Shadowless Boundary Extraction

To focus on the edge of the target object and reduce the rest of the information, we generate a binary image. Image binarization is thereby performed in such a way that the edge of the

target object is set to 1 (white) and the rest of the information (shadow, noise, and background), on the other hand, is set to 0 (black). Thus, the generated edge here represents the shadowless boundary of the target object. Image binarization f_{ed} thus is given as

$$\forall f \geq T_1, f_{ed} = 1,$$
$$\forall f \geq T_1, f_{ed} = 0.$$

Where f_{ed} represents the detected edge, and T_1 represents a threshold value that separates the boundary of the shadowless object and the rest information of the image. This boundary is then delivered to the next stage, in which the (ROI) is blurred and highlighted.

2.4. Highlighting the Region of Interest

In this stage, the region representing the shadowless object was highlighted, as it is referred to as the (ROI). As mentioned previously, the binary image contains the edge of the shadowless object and ignores the rest of the information. As a consequence, the ROI, here, represents the interior of the generated boundary and thus represents the body of the shadowless object in the visual scene. The spatial ROI is blurred and highlighted based on the 2D bell shape function g. Consequently, the ROI is described by $I = g * f_{ed}$, in which '*' denotes the convolution operator, $g = \frac{1}{2\pi\sigma^2} \exp -\frac{x^2+y^2}{2\sigma^2}$, and σ is the spatial extent of the 2D bell shape function. The blurred ROI is then delivered to the next stage, in which the target object is reconstructed in a shadowless image.

2.5. Shadowless Object Reconstruction

In this stage, the shadowless object and image background are reconstructed in a new image. The new image P, thus combines the shadowless object and the image background, as defined by

$$\forall I \geq T_2, P_{ij} = I_{ij}$$
$$\forall f_{bak} < T_2, P_{ij} = f_{bak_{ij}}$$

Where T_2 denotes a threshold value (i, j) represent the spatial coordinates in the 2D space of the original image I and background image f_{bak}.

3. Intensity Distribution of Shadow Regions

To investigate the intensity distribution in images that include shadow regions, Fig. 2 shows the intensity of the three scenes. The first column shows the original images with the shadow region, see(a1-a3). The second column (b1-b3) illustrates the foreground part of the images. Here, the foreground of the images is defined by

$$\forall F_{x,y} \leq mu, I_{x,y}^{for} = F_{x,y}.$$

The mu represents the threshold value that separates the foreground and the background. In our implementation the value of foreground separation is mu =60.

The intensity distribution of the relative images is shown in Fig. 3, where the x-axis represents the intensity values, and the y-axis represents the number of pixels. These plots reflect the distribution of the intensities for the foreground images. The plot reveals that the intensity of the foreground images (object) merited a small area of intensity as highlighted the third column in Fig. 2. However, shadow and noise are spread over a larger region of intensity. Since the foreground image has a monochrome background (white), the intensity value (255) covers the highest number of pixels. As a consequence, the target object is separated from the shadows and noise, as defined by

$$\forall I_{x,y}^{for} \leq k, I_{x,y}^{object} = I_{x,y}^{for}.$$

Where k represents the shadowless separation value. In our implementation, the value of k is set to 60. To keep the object same size as the shadowless objects, we represent the shadowless object on a black background as shown in the third column (d1-d3) in Fig. 2. The results reveal that the shadow intensity in many cases can be separated from the target object based

on the distribution of the image intensity. However, the separation value of the shadowless object is a critical issue and depend on the lighting conditions, and thus different values could be selected for the other databases.

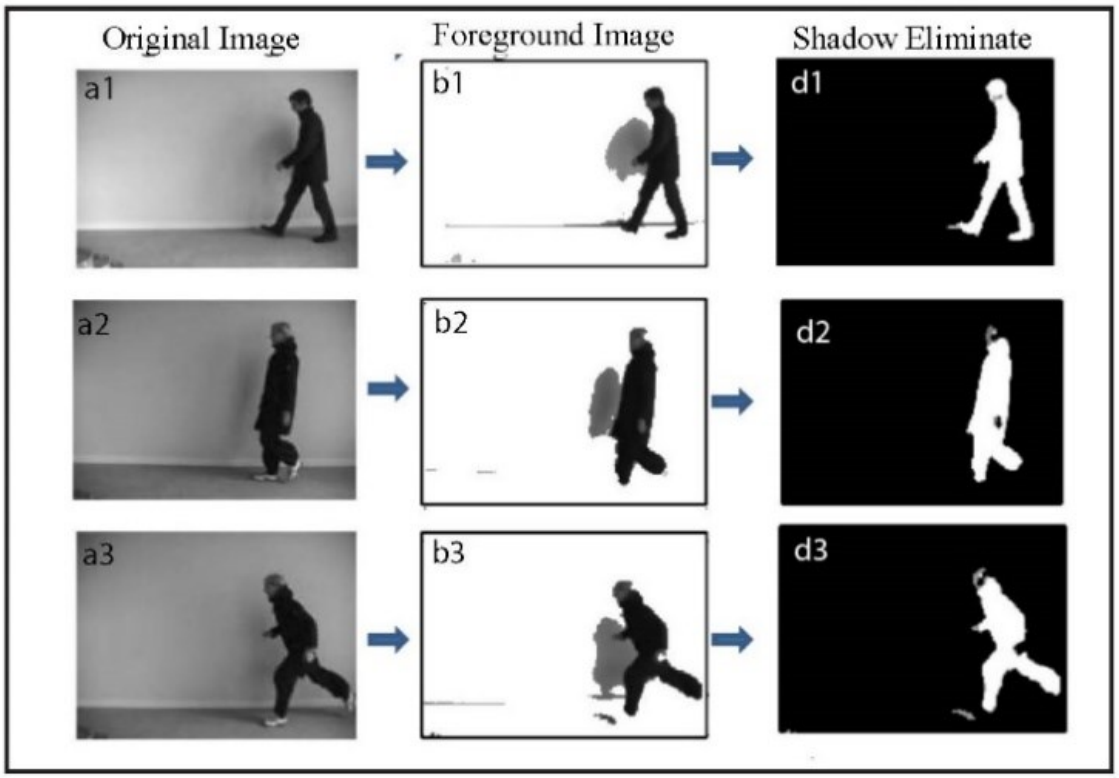

Fig.2 Intensity distributions in different images. The first column (a1-a3) shows the original images with shadow regions. The second column (b1-b3) illustrates the foreground of the images. The third column (d1-d3) represent the shadowless object on a black background.

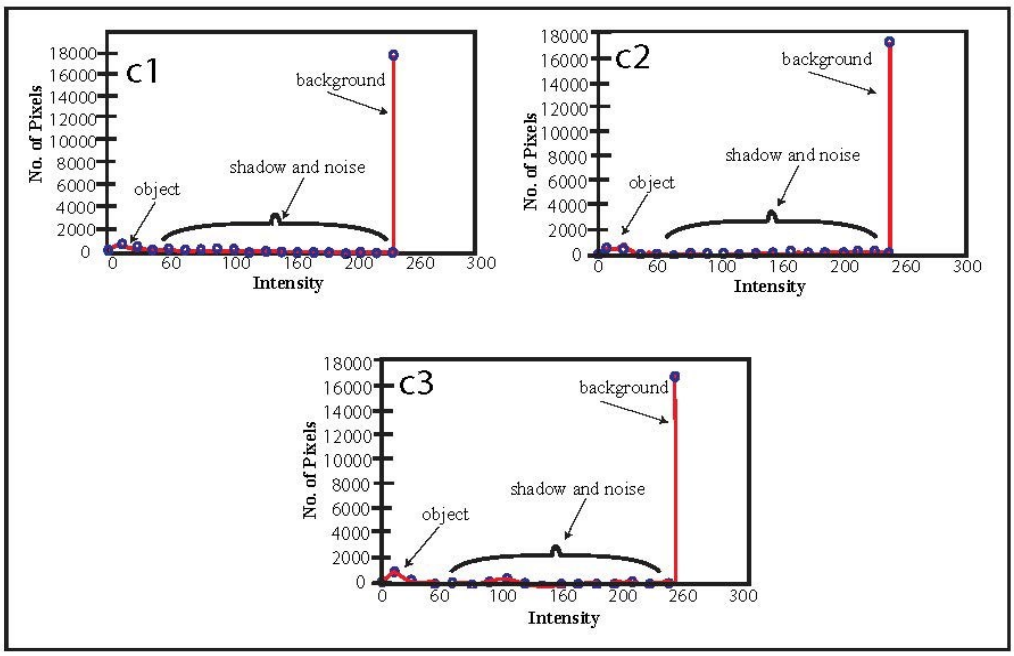

Fig.3 The distribution of the intensities for the foreground images. The x-axis represents the intensity values, and the y-axis represents the number of pixels.

4. Results and Discussion

To evaluate the performance of our mechanism, we tested it with realistic scenarios that contain self-shadows (i.e., shadows linked with objects). Since in the future we plan to focus on human action recognition as an extended work, we used the KTH database [28]. The KTH database is characterized as complex scenarios with shadows around the target objects in different locations. This dataset provides a valuable benchmark for evaluating shadow detection and elimination methods. In our evaluation, different subjects with different scenes are addressed. In addition, this database has a relatively low resolution, making detecting shadows complex. Since the scenarios of the KTH database contain moving objects, we used the background subtraction technique to extract these objects [29]. Here, the median value of constitutive frames is considered as a background of the scenario $I_{x,y} = median\{ F_{x,y,t}\}$. Where t ∈ {1, 2, ...m} and m denotes the number of frames used for background subtraction. Following the suggestion of [30], we restored the designated scene with static backgrounds, ∀ (F_(x,y)-I_(x,y)) < d, I_(x,y) = F_(x,y), where d represents a small value that describes the disparity between the background I and the foreground F.

Table 1 presents the parameters of the proposed model. In our performance, the shortest length of the dataset scenarios is used (see [31]), and as a consequence, the number of frames used for background subtraction is m=28. The size of the Gaussian derivative kernels (gx, gy) is (40 × 40) in which the spatial extent σx_1, σy_1 are 3, 5 and the spatial extent σx_2, σy_2 are 5, 3, respectively. The relative disparity of the foreground and background value is d=50. The values of the threshold parameters are T_1, T_2 are 0.5, 0.2, respectively. In the normalizing process, the size of the Gaussian window Λ in the spatial domain is (49 × 49) in which the value of σ is 10 and the value of ε is 0.3.

TABLE I Parameters used in our model.

Definition	variable	value
The number of frames used for background subtraction	m	28
Gaussian derivative kernels	(gx, gy)	(40 × 40)
spatial extent	σx_1, σy_1, σx_2, σy_2	3, 5, 5, 3
The relative disparity of the foreground and background value	d	50
Threshold parameters	T_1, T_2	0.5, 0.2
The size of the Gaussian window	Λ	(49 × 49)
Normalizing parameter	ε	0.3

We examined the performance of our model by probing it with the KTH database. We selected several scenes from the KTH database with different subjects. As previously mentioned, our mechanism aims to eliminate the shadow from an image and to reconstruct it as a shadowless image. Here, we focus on the scenes that contain shadows and select different indoor and outdoor scenarios. These scenarios include different scenes and, moving objects escorted by shadows appearing in different directions. Fig. 4 shows four images from indoor

scenarios of the KTH dataset. As mentioned in Section 2, the shadow was detected and eliminated from the image using four stages. Fig. 4 shows the results of the four processing stages in which each row represents one of the selected images (with a coherent shadow), and each column shows the results of the proposed stages. Here, the first column ((a1-a4)-in) shows the (origin) images that contain shadows, and the second column ((b1-b4)-in), on the other hand, presents the detected contour of the target object. The third column ((c1-c4)-in) shows the highlighted ROI. Finally, the fourth column ((d1-d4)-in) shows the reconstruction of the shadowless images. By way of illustration, the eliminated shadows in the fourth column of Fig. 4 are circled. The results reveal that our mechanism can detect and eliminate the shadows from indoor images and reconstruct them as shadowless images. To verify the robustness of our mechanism for the shadow removal from outdoor images, we tested our mechanism with several outdoor images from the KTH dataset as shown in Fig. 5. We selected three scenarios containing shadows from the outdoor database. These scenarios were probed through the suggested consecutive stages in which the results of each stage are shown in the relative column in Fig. 5. The first column ((a1-a3)-out) shows the original scenes of the selected scenarios, while the second and third columns ((b1-b3)-out) and ((c1-c2)-out) show the edge detection and the highlighted ROI, respectively. The shadowless images are reconstructed in the fourth column ((d1-d3)-out). Again, the regions of the eliminated shadows are circled in the fourth column in Fig. 5. The results show that our mechanism is able to detect and eliminate the shadows from outdoor scenes and reconstruct images into shadowless images.

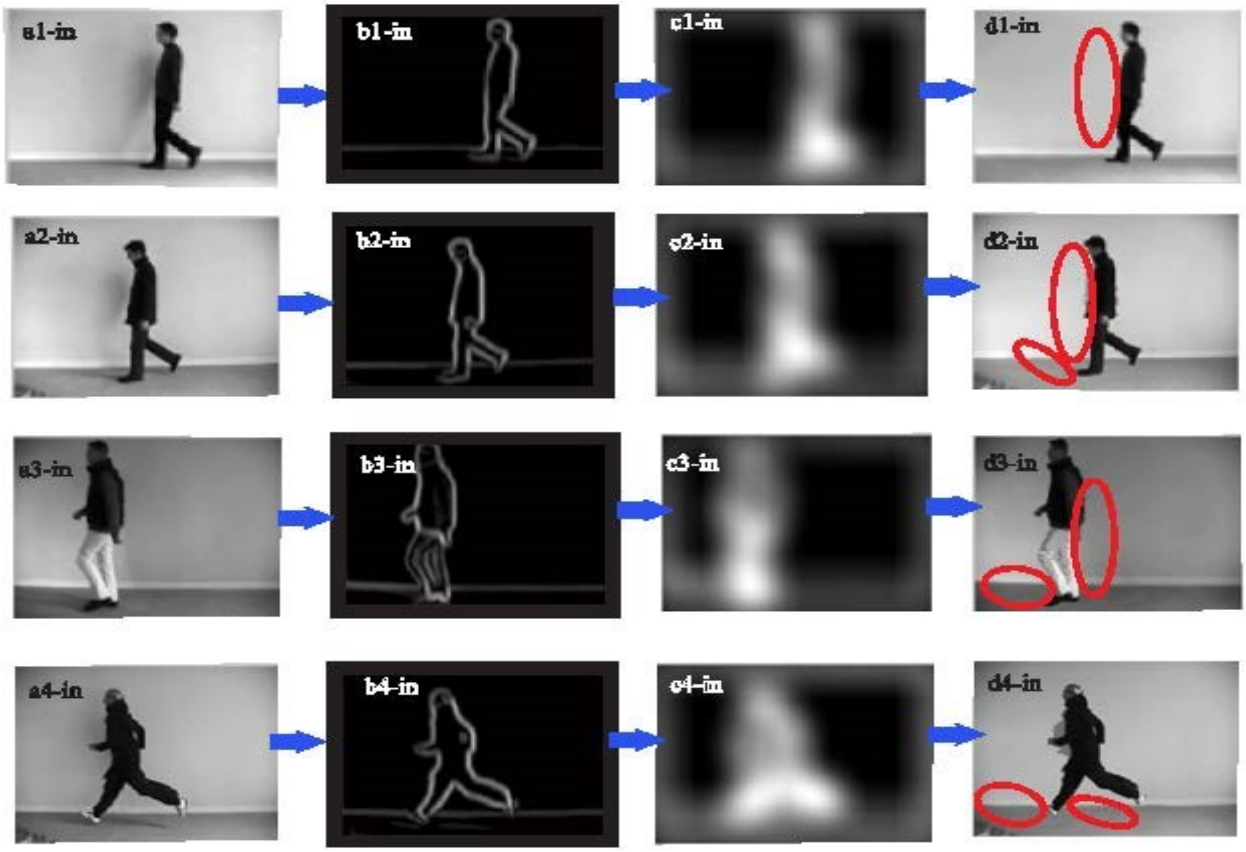

Fig. 4 Indoor images of the KTH dataset. The first column ((a1-a4)-in) shows the (original) images that contain shadows, and the second column ((b1-b4)-in) presents the detected contour of the target object. The third column ((c1-c4)-in) demonstrates the highlighted ROI. The fourth column ((d1-d4)-in) shows the reconstruction of the shadowless images in which the regions of the eliminated shadows are circled.

In order to measure the accuracy of the shadow removal approach, we calculated the total error, e_t, which is determined by

$$e_t = \sum_{i=1}^{n} e_i \,,$$
$$e_i = \frac{N_i}{M_i} \,.$$

Where $e_t$represents the summation of the error values for {i = 1...n} in which n denotes the number of images, $e_i$represents the error of the shadow removal for image i and Ni denotes the number of pixels freed from the shadows in image i and M_i represents the number of shadow pixels in the related image i (origin image). The results show that the total error of our approach is 6%, which reflects its ability to detect and remove the shadow regions from indoor and outdoor scenarios.

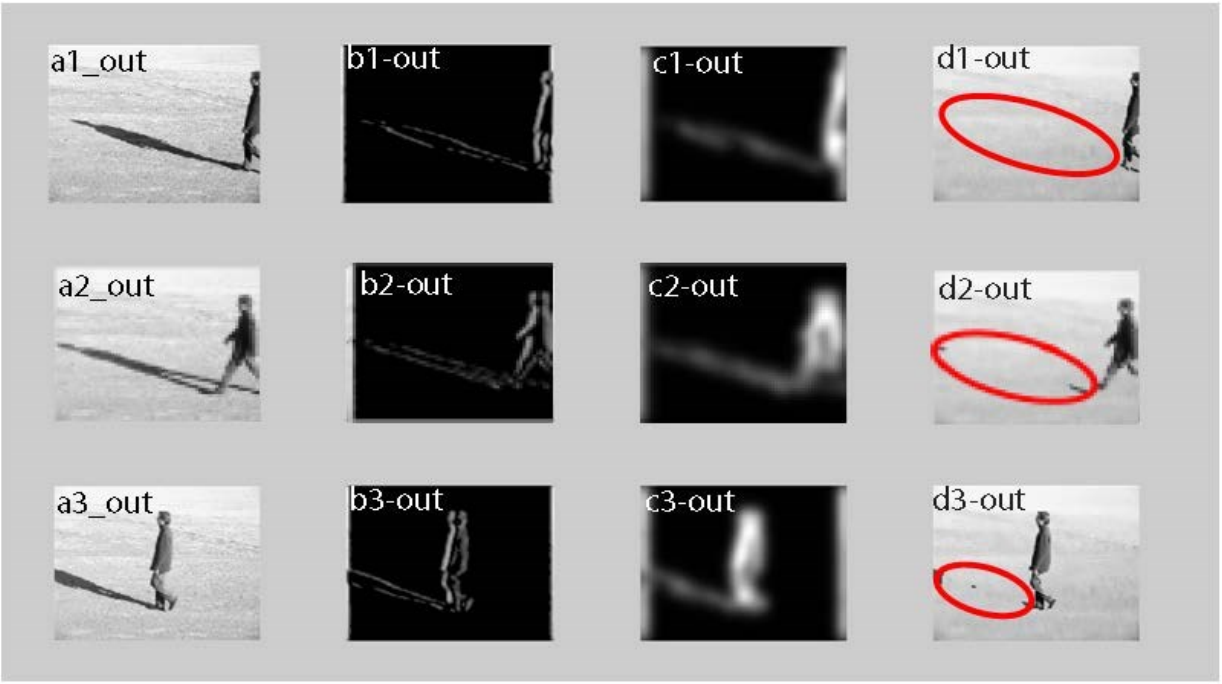

Fig. 5 Outdoor images of the KTH dataset. The first column ((a1-a4)-out) shows the (original) images that contain shadows, and the second column ((b1-b4)-out) presents the detected contour of the target object. Third column ((c1-c4)-out) demonstrates the highlighted ROI. The fourth column ((d1-d4)-out) shows the reconstruction of the shadowless images in which the regions of the eliminated shadows are circled.

5. Conclusions

We have presented a mechanism for shadow detection and removal. The mechanism is organized in a cascade of five consecutive processing stages. Contrast filtering is performed in the first stage, followed by normalization of the obtained result in the second stage. Next, edge extraction is conducted in the third stage to detect the contour of the target object. In order to reconstruct the target object in a shadowless image, the interior of the object is highlighted in the fourth stage and reconstructed in the fifth stage. The results demonstrate that the proposed processing stages enable the detection and elimination of shadow regions from an image

The distribution of the image intensity was investigated and the potential of shadow elimination based on intensity distributions has been described. In addition, the distribution of the image intensity can give an indication regarding the elements in the scene (i.e. object, shadow, and background). However, the distribution of the image intensity is affected by several factors such as image resolution and light conditions. As a consequence, the intensity of the scene (object and shadow) differs from image to image depending on the adopted database.

To demonstrate the robustness of the proposed stages to detect and element the shadows from certain images, we used the KTH database that contains different scenarios (indoors and outdoors) where we focused on the images that contained shadows. The results reflect the robustness of our approach for shadow detection and removal with an error of 6%.

This approach can be extended to address shadow detection and removal in high-resolution colored images by analyzing and visualizing the distribution of the RGB intensity using different levels of data filtering. In addition, this approach can be used for different applications for more than one object. Our current study exploits the generated shadow-less images for human action recognition.

Acknowledgment

We would like to thank Prof. Heiko Neumann for his support and help. We would also like to thank the institute of Neural Information Processing at Ulm university.

References

1. K. Karsch et al., “Automatic Scene Inference for 3D Object Compositing.” arXiv, Dec. 24, 2019. doi: 10.48550/arXiv.1912.12297.

2. T. Okabe, I. Sato, and Y. Sato, “Attached shadow coding: Estimating surface normals from shadows under unknown reflectance and lighting conditions,” in 2009 IEEE 12th International Conference on Computer Vision, Kyoto: IEEE, Sep. 2009, pp. 1693–1700. doi: 10.1109/ICCV.2009.5459381.

3. R. Cucchiara, C. Crana, M. Piccardi, A. Prati, and S. Sirotti, “Improving shadow suppression in moving object detection with HSV color information,” in ITSC 2001. 2001 IEEE Intelligent Transportation Systems. Proceedings (Cat. No.01TH8585), Oakland, CA, USA: IEEE, 2001, pp. 334–339. doi: 10.1109/ITSC.2001.948679.

4. L. I. Abdul-Kreem and H. Neumann, “Estimating visual motion using an event-based artificial retina,” in Imaging and Computer Graphics Theory and Applications, in Series of CCIS Communications in Computer and Information Science. Computer Vision. Springer International Publishing Switzerland, 2016, pp. 396–415.

5. L. I. Abdul-Kreem and H. K. Abdul-Ameer, “Object tracking using motion flow projection for pan-tilt configuration,” Int. J. Electr. Comput. Eng. IJECE, vol. 10, no. 5, p. 4687, Oct. 2020, doi: 10.11591/ijece.v10i5.pp4687-4694.

6. R. K. Sasi and V. K. Govindan, “Shadow Detection and Removal from Real Images: State of Art,” in Proceedings of the Third International Symposium on Women in Computing and Informatics - WCI ’15, Kochi, India: ACM Press, 2015, pp. 309–317. doi: 10.1145/2791405.2791450.

7. C. M., G. R., V. T., and A. C.B., “Cast and Self Shadow Segmentation in Video Sequences using Interval based Eigen Value Representation,” Int. J. Comput. Appl., vol. 142, no. 4, pp. 27–32, May 2016, doi: 10.5120/ijca2016909752.

8. . Xu, J. Liu, X. Li, Z. Liu, and X. Tang, “Insignificant shadow detection for video segmentation,” IEEE Trans. Circuits Syst. Video Technol., vol. 15, no. 8, pp. 1058–1064, Aug. 2005, doi: 10.1109/TCSVT.2005.852402.

9. L. Hou, T. F. Y. Vicente, M. Hoai, and D. Samaras, “Large Scale Shadow Annotation and Detection Using Lazy Annotation and Stacked CNNs,” IEEE Trans. Pattern Anal. Mach. Intell., vol. 43, no. 4, pp. 1337–1351, Apr. 2021, doi: 10.1109/TPAMI.2019.2948011.

10. Q. Zheng, X. Qiao, Y. Cao, and R. W. H. Lau, “Distraction-Aware Shadow Detection,” in 2019 IEEE/CVF Conference on Computer Vision and Pattern Recognition (CVPR), Long Beach, CA, USA: IEEE, Jun. 2019, pp. 5162–5171. doi: 10.1109/CVPR.2019.00531.

11. W. Xu et al., “Shadow detection and removal in apple image segmentation under natural light conditions using an ultrametric contour map,” Biosyst. Eng., vol. 184, pp. 142–154, Aug. 2019, doi: 10.1016/j.biosystemseng.2019.06.016.

12. H. K. Suh, J. W. Hofstee, and E. J. van Henten, “Improved vegetation segmentation with ground shadow removal using an HDR camera,” Precis. Agric., vol. 19, no. 2, pp. 218–237, Apr. 2018, doi: 10.1007/s11119-017-9511-z.

13. J. Wang, X. Li, and J. Yang, “Stacked Conditional Generative Adversarial Networks for Jointly Learning Shadow Detection and Shadow Removal,” in 2018 IEEE/CVF Conference on Computer Vision and Pattern Recognition, Salt Lake City, UT: IEEE, Jun. 2018, pp. 1788–1797. doi: 10.1109/CVPR.2018.00192.

14. S. K. Yarlagadda et al., “Shadow Removal Detection and Localization for Forensics Analysis,” in ICASSP 2019 - 2019 IEEE International Conference on Acoustics, Speech and Signal Processing (ICASSP), May 2019, pp. 2677–2681. doi: 10.1109/ICASSP.2019.8683695.

15. Y. Ke, F. Qin, W. Min, and G. Zhang, “Exposing Image Forgery by Detecting Consistency of Shadow,” Sci. World J., vol. 2014, pp. 1–9, 2014, doi: 10.1155/2014/364501.

16. D. Hutchison et al., “Detecting Ground Shadows in Outdoor Consumer Photographs,” in Computer Vision – ECCV 2010, K. Daniilidis, P. Maragos, and N. Paragios, Eds., in Lecture Notes in Computer Science, vol. 6312. Berlin, Heidelberg: Springer Berlin Heidelberg, 2010, pp. 322–335. doi: 10.1007/978-3-642-15552-9_24.

17. C. C. Newey, O. D. Jones, and H. M. Dee, “Shadow detection for mobile robots: Features, evaluation, and datasets,” Spat. Cogn. Comput., vol. 18, no. 2, pp. 115–137, Apr. 2018, doi: 10.1080/13875868.2017.1322088.

18. R. Guo, Q. Dai, and D. Hoiem, “Paired Regions for Shadow Detection and Removal,” IEEE Trans. Pattern Anal. Mach. Intell., vol. 35, no. 12, pp. 2956–2967, Dec. 2013, doi: 10.1109/TPAMI.2012.214.

19. L. Qu, J. Tian, S. He, Y. Tang, and R. W. H. Lau, “DeshadowNet: A Multi-context Embedding Deep Network for Shadow Removal,” in 2017 IEEE Conference on Computer Vision and Pattern Recognition (CVPR), Honolulu, HI: IEEE, Jul. 2017, pp. 2308–2316. doi: 10.1109/CVPR.2017.248.

20. N. Inoue and T. Yamasaki, “Learning From Synthetic Shadows for Shadow Detection and Removal,” IEEE Trans. Circuits Syst. Video Technol., vol. 31, no. 11, pp. 4187–4197, Nov. 2021, doi: 10.1109/TCSVT.2020.3047977.

21. Shao-Yi Chien, Shyh-Yih Ma, and Liang-Gee Chen, “Efficient moving object segmentation algorithm using background registration technique,” IEEE Trans. Circuits Syst. Video Technol., vol. 12, no. 7, pp. 577–586, Jul. 2002, doi: 10.1109/TCSVT.2002.800516.

22. L. Zhang, Q. Zhang, and C. Xiao, “Shadow Remover: Image Shadow Removal Based on Illumination Recovering Optimization,” IEEE Trans. Image Process., vol. 24, no. 11, pp. 4623–4636, Nov. 2015, doi: 10.1109/TIP.2015.2465159.

23. X. Fan et al., “Shading-aware shadow detection and removal from a single image,” Vis. Comput., vol. 36, no. 10–12, pp. 2175–2188, Oct. 2020, doi: 10.1007/s00371-020-01916-3.

24. X. Hu, C.-W. Fu, L. Zhu, J. Qin, and P.-A. Heng, “Direction-Aware Spatial Context Features for Shadow Detection and Removal,” IEEE Trans. Pattern Anal. Mach. Intell., vol. 42, no. 11, pp. 2795–2808, Nov. 2020, doi: 10.1109/TPAMI.2019.2919616.

25. T. Wang, X. Hu, Q. Wang, P.-A. Heng, and C.-W. Fu, “Instance Shadow Detection,” in 2020 IEEE/CVF Conference on Computer Vision and Pattern Recognition (CVPR), Seattle, WA, USA: IEEE, Jun. 2020, pp. 1877–1886. doi: 10.1109/CVPR42600.2020.00195.

26. L. I. Abdul-Kreem and H. Neumann, “Neural Mechanisms of Cortical Motion Computation Based on a Neuromorphic Sensory System,” PLOS ONE, vol. 10, no. 11, p. e0142488, Nov. 2015, doi: 10.1371/journal.pone.0142488.

27. L. I. Abdul-Kreem and H. Neumann, “Bio-inspired Model for Motion Estimation using an Address-event Representation:”, in Proceedings of the 10th International Conference on Computer Vision Theory and Applications, Berlin, Germany: SCITEPRESS - Science and and Technology Publications, 2015, pp. 335–346. doi: 10.5220/0005311503350346.

28. C. Schuldt, I. Laptev, and B. Caputo, “Recognizing human actions: a local SVM approach,” in Proceedings of the 17th International Conference on Pattern Recognition, 2004. ICPR 2004., Cambridge, UK: IEEE, 2004, pp. 32-36 Vol.3. doi: 10.1109/ICPR.2004.1334462.

29. C. Stauffer and W. E. L. Grimson, “Adaptive background mixture models for real-time tracking,” in Proceedings. 1999 IEEE Computer Society Conference on Computer Vision and Pattern Recognition (Cat. No PR00149), Fort Collins, CO, USA: IEEE Comput. Soc, 1999, pp. 246–252. doi: 10.1109/CVPR.1999.784637.

30. L. I. Abdul-Kreem, “Computational architecture of a visual model for biological motions segregation,” Netw. Comput. Neural Syst., vol. 30, no. 1–4, pp. 58–78, Oct. 2019, doi: 10.1080/0954898X.2019.1655173.

31. K. Schindler and L. van Gool, “Action snippets: How many frames does human action recognition require?”, in 2008 IEEE Conference on Computer Vision and Pattern Recognition, Anchorage, AK, USA: IEEE, Jun. 2008, pp. 1–8. doi: 10.1109/CVPR.2008.4587730.